nature energy

SUPPLEMENTARY INFORMATION

https://doi.org/10.1038/s41560-019-0349-7

In the format provided by the authors and unedited.

Solid-state polymer electrolytes with in-built fast interfacial transport for secondary lithium batteries

Qing Zhao[1], Xiaotun Liu[1], Sanjuna Stalin[1], Kasim Khan[1] and Lynden A. Archer[1,2]*

[1]Robert Frederick Smith School of Chemical and Biomolecular Engineering, Cornell University, Ithaca, NY, USA. [2]Department of Materials Science and Engineering, Cornell University, Ithaca, NY, USA. *e-mail: laa25@cornell.edu

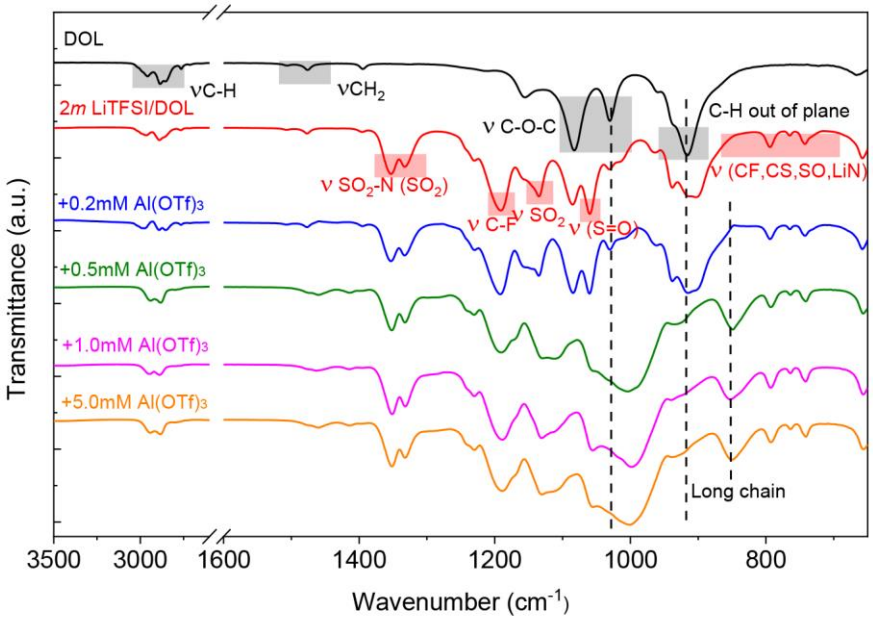

Supplementary Fig.1 | ATR-FTIR spectra of pure DOL, liquid DOL electrolyte (2 *m* LiTFSI/DOL) and poly-DOL electrolyte with different concentration of $Al(OTf)_3$. Various peaks belong to the vibrations of LiTFSI and DOL are detected for liquid electrolyte.[1-3] The electrolyte with 0.2mM $Al(OTf)_3$ still show similar profiles as liquid electrolyte. Then the SPE is generated after increasing the concentrations of $Al(OTf)_3$ higher than 0.5mM. The position change of –O-C- vibration, the missing of C-H out of plane vibration and the emerging of chain vibration indicate the polymerization of DOL.[3]

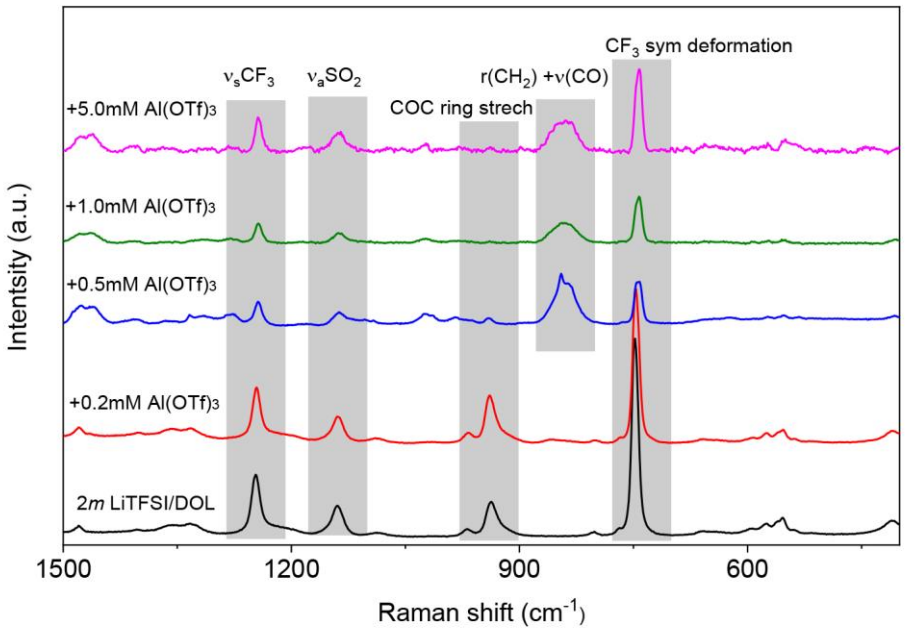

Supplementary Fig.2 | Raman spectra of pure DOL, liquid DOL electrolyte (2 *m* LiTFSI/DOL) and poly-DOL electrolyte with different concentration of $Al(OTf)_3$. The results of Raman spectra are consistent with FTIR spectra. Typical peaks of CF_3, SO_3 can be detected for all the electrolytes.[4,5] After increasing the concentration of $Al(OTf)_3$ to 0.5mM, the ring stretch belong to DOL are dismissed. Meanwhile, the vibration of C-O and CH_2 belong to linear poly-DOL polymer appeared, indicating the polymerization of DOL.[6]

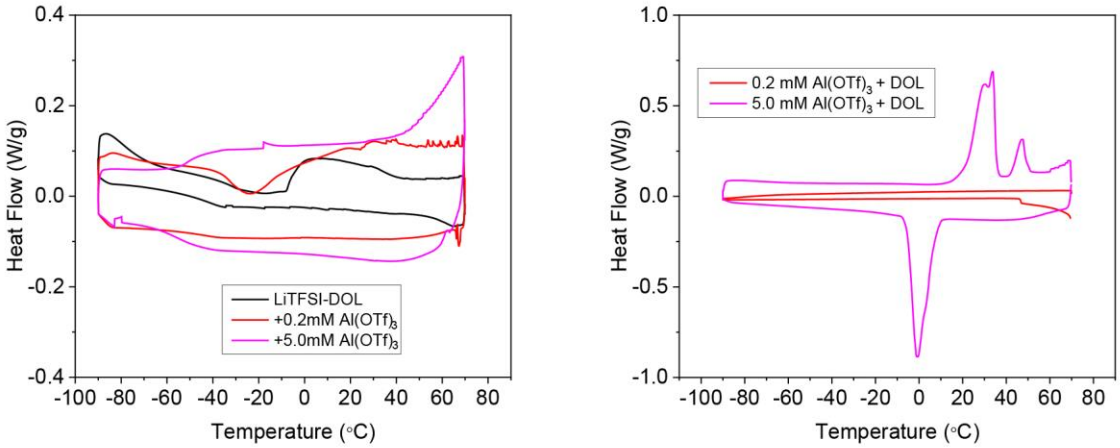

Supplementary Fig.3 | DSC analysis of (a) poly-DOL electrolyte and (b) poly-DOL solvent. The DOL electrolyte and DOL solvent with lower $Al(OTf)_3$ catalyst (0.2 mM) solvent display liquid like behaviors. For solid state DOL electrolyte, we found small peaks and pits observed in the temperature range 0~60 °C associated with melting behavior (for electrolyte with 0.5mM $Al(OTf)_3$) and there are no corresponding crystallization peaks. This behavior is inconsistent with normal observations for semicrystalline polymers and clearly at odds with what is observed for the LiTFSI-free poly-DOL SPE; we attribute it here to interactions between long-chain polymer and LiTFSI salt.

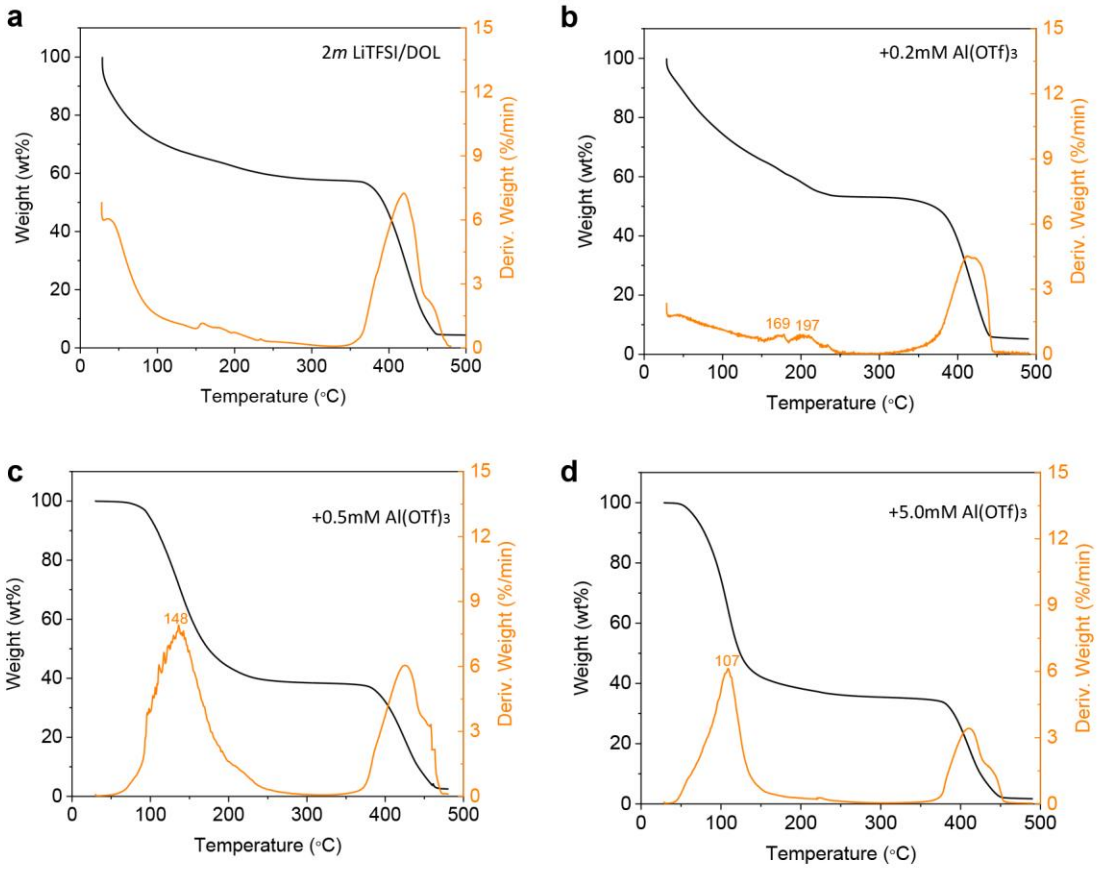

Supplementary Fig.4 | TGA profiles of different electrolytes. (a) 2m LiTFSI/DOL; (b) adding 0.2mM $Al(OTf)_3$; (b) adding 0.5mM $Al(OTf)_3$; (b) adding 5.0 mM $Al(OTf)_3$. The decomposition of LiTFSI occurs at about 400 °C.[7] Due to the low boiling points of DOL (75 °C), the liquid like electrolyte (2m LiTFSI/DOL, 0.2mM+2m LiTFSI/DOL) will lose weight even at room-temperature. The thermal stability increased for poly-DOL SPE. After increasing temperature, the decomposition temperature decrease due to the reduction of molecular weight.

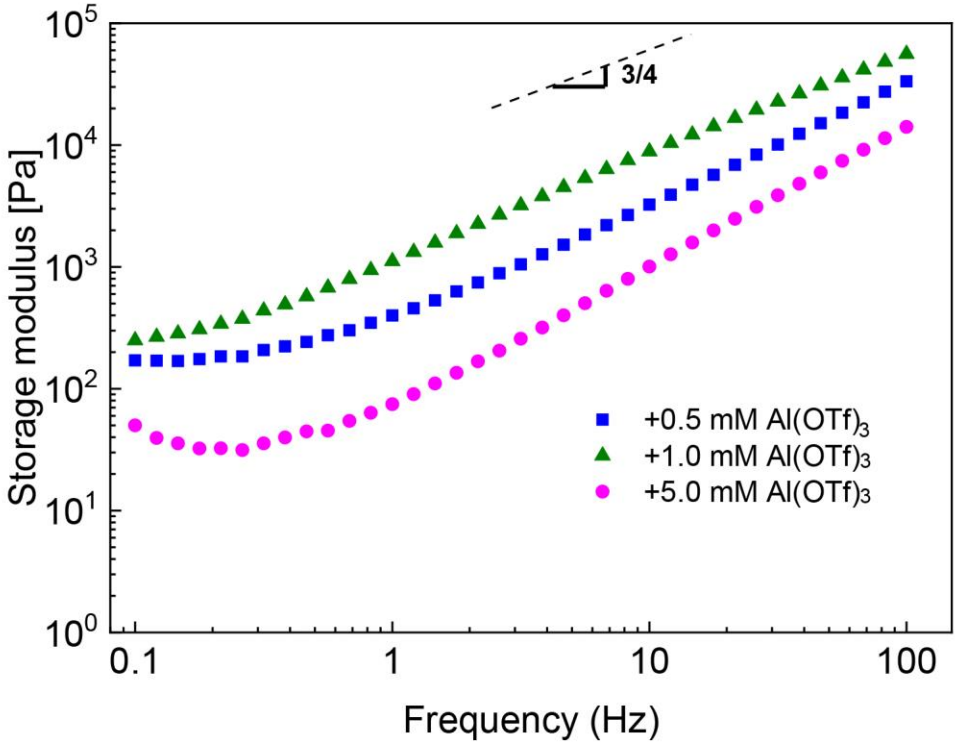

Supplementary Fig.5 | Oscillatory shear response of poly-DOL SPE from SAOS measurements. The materials has a higher storage modulus G′ and is thus more solid-like at intermediate Al^{3+} concentration (0.5mM, 1mM). The figure further shows that over a wide range of shear frequencies, G′ follows a sub-linear power-law relationship $G' \sim \omega^{3/4}$, which ultimately gives way to a frequency-independent plateau at low ω. This behavior is typical of materials in the dynamic universal class viscoelastic solids, it provides fundamental support for their classification as solid-state polymer electrolytes.

.

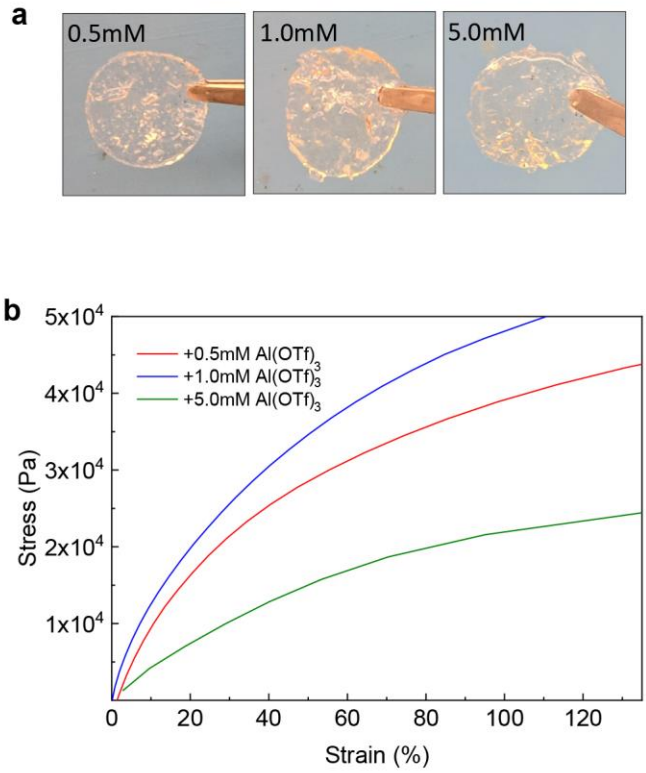

Supplementary Fig.6 | (a) Digital images of ex-situ synthesized SPE at different $Al(OTf)_3$ compositions. (b) Stress-strain of prepared free-standing poly-DOL electrolyte. The poly-DOL SPE can be ex-situ made as flexible and free-standing membrane with transparent color. The SPEs exist as free-standing elastic materials for which Young's modulus E (slope of longitudinal stress vs. strain) also varies in a non-monotonic fashion with Al^{3+} concentration. The results of Supplementary Fig.5 and Fig.6 demonstrate that a higher molecular weight tends to enhance the elasticity of the material, and a larger residual monomer content softens the material (see Supplementary Table 1), which together results in the oscillatory shear response and stress-strain behavior.

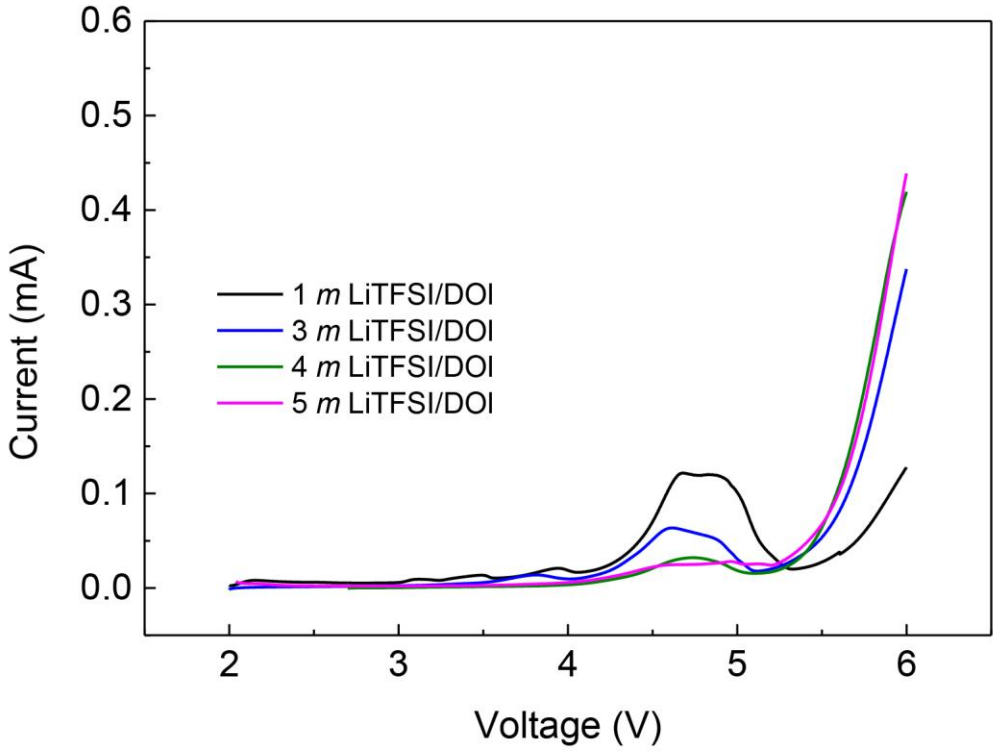

Supplementary Fig.7 | linear sweep of liquid DOL with different concentration of LiTFSI as a sweep rate of 1mV/s. The voltage stability window of liquid LiTFSI/DOL electrolyte can be slightly improved after increasing LiTFSI concentration.

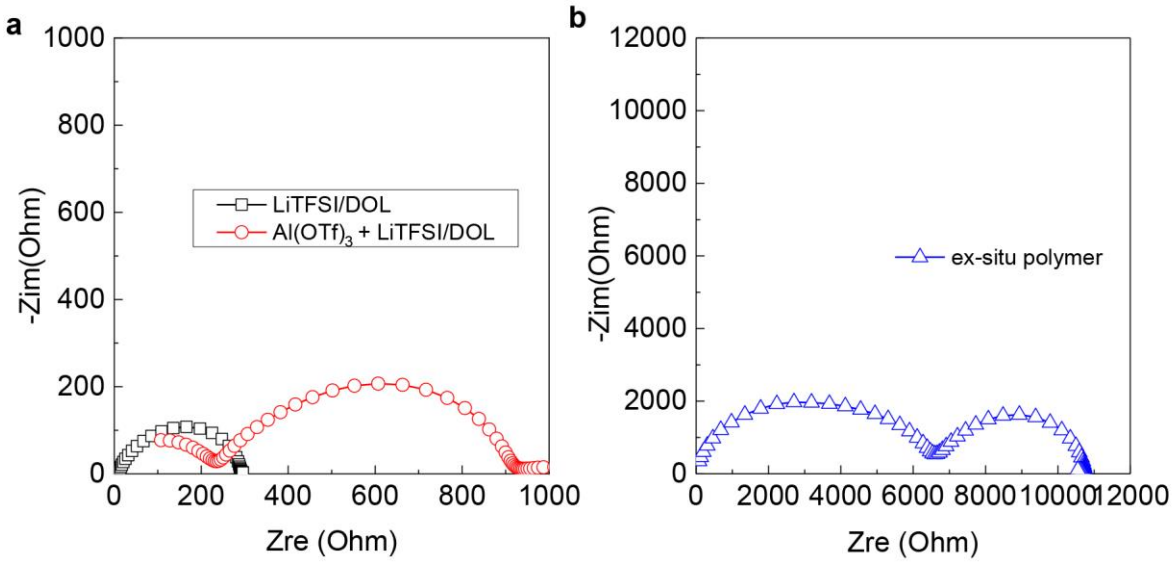

Supplementary Fig.8 | EIS of symmetrical Li cells using (a) liquid electrolyte, In-situ SPE and (b) ex-situ SPE. EIS of symmetrical Li cell with liquid electrolyte was measured using 2 *m* LiTFSI/DOL. The cell with in situ SPE was measured using 0.5mM Al^{3+} + 2 *m* LiTFSI/DOL electrolyte that polymerized inside the batteries. For symmetrical Li cells using ex-situ polymer electrolyte, the electrolyte (also 0.5mM Al^{3+} + 2 *m* LiTFSI/DOL) was firstly prepared in glove box, and used to assemble symmetrical cell.

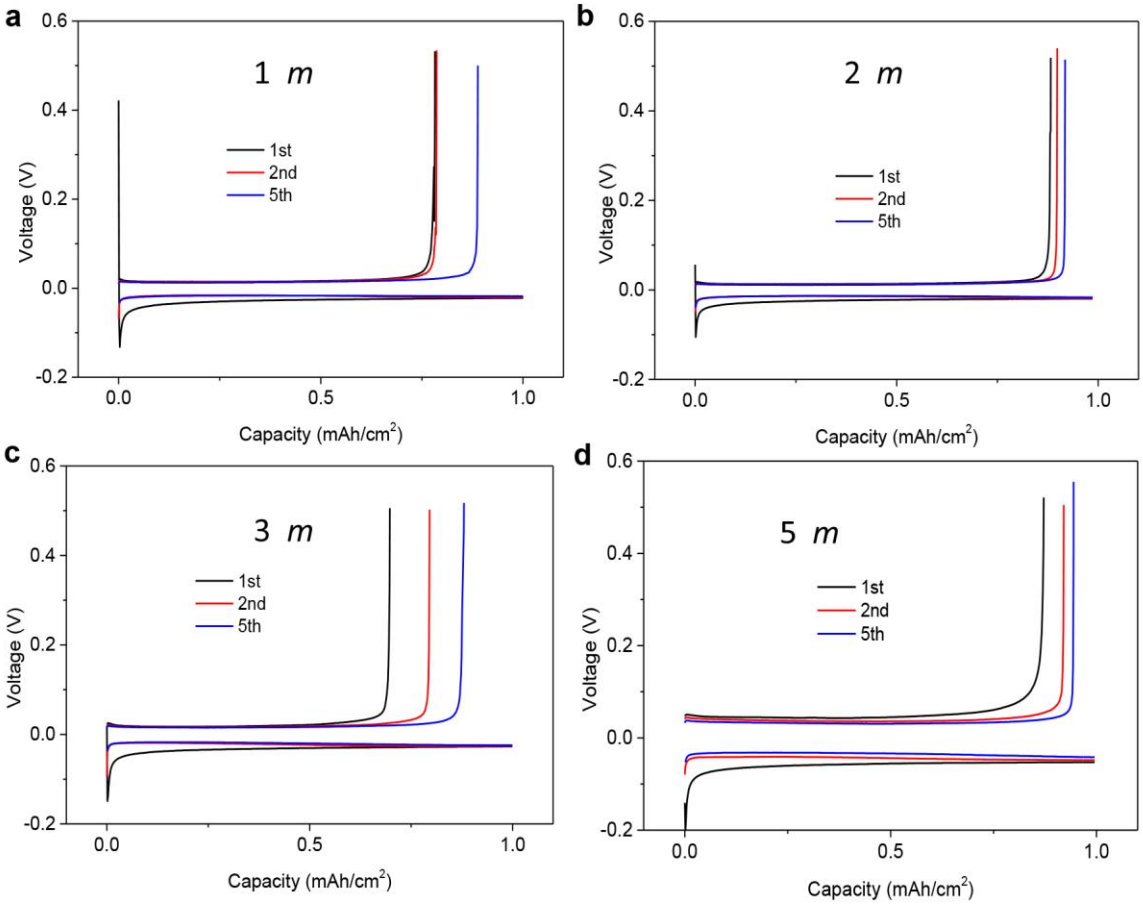

Supplementary Fig.9 | Li stripping and plating properties of Li-Cu cells using liquid LiTFSI/DOL electrolytes with different LiTFSI concentrations. (a) 1 *m* LiTFSI/DOL; (b) 2 *m* LiTFSI/DOL; (c) 3 *m* LiTFSI/DOL; (d) 5 *m* LiTFSI/DOL. The current density is 1 mA/cm^2 and the plating Li capacity is 1mAh/cm^2 per cycle.

.

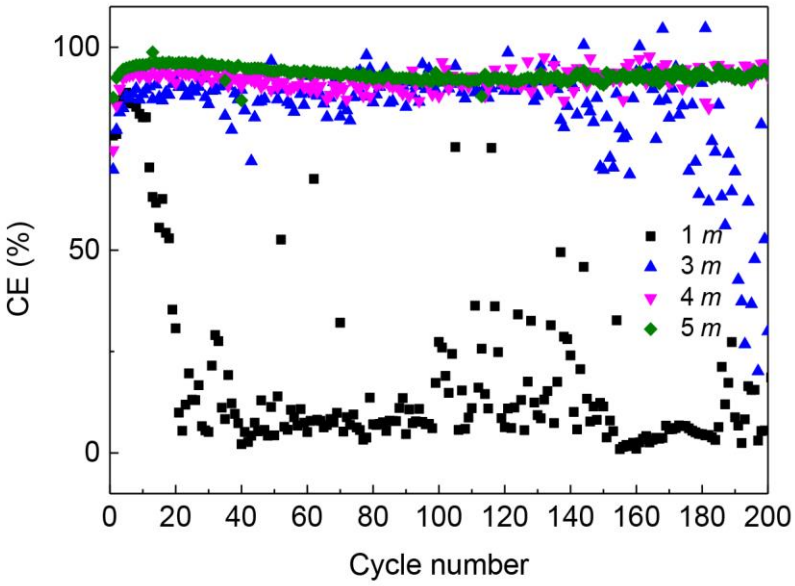

Supplementary Fig.10 | Coulombic efficiencies of Li-Cu batteries using liquid LiTFSI-DOL electrolytes. The current density is 1 mA/cm^2 and the plating Li capacity is 1mAh/cm^2 per cycle.

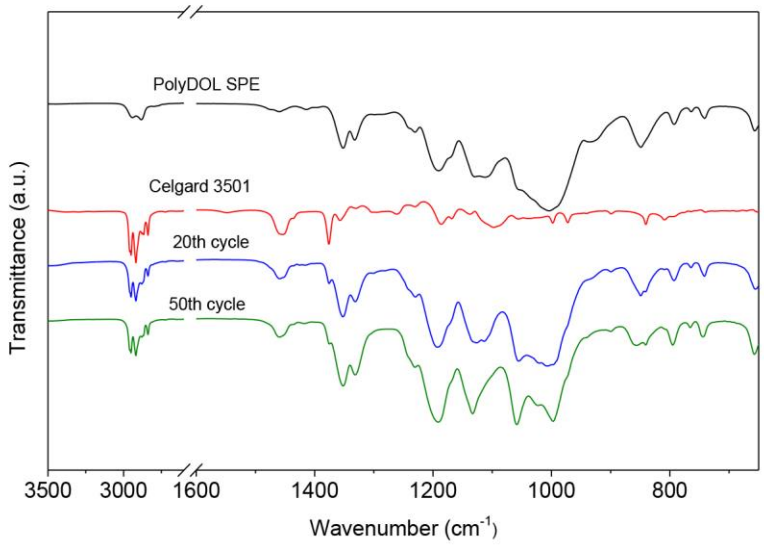

Supplementary Fig.11 |FTIR spectra of cycled poly-DOL SPE in symmetrical cells.

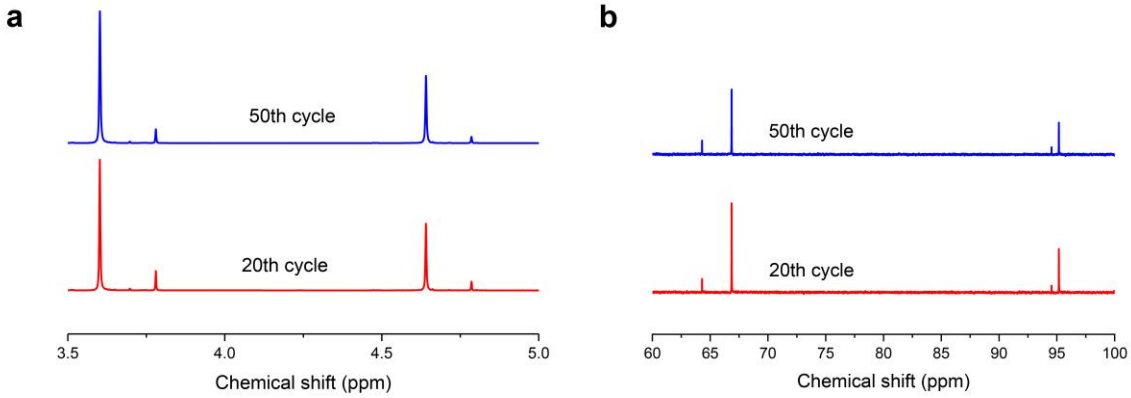

Supplementary Fig.12 | NMR spectra of cycled poly-DOL SPE in symmetrical cells.

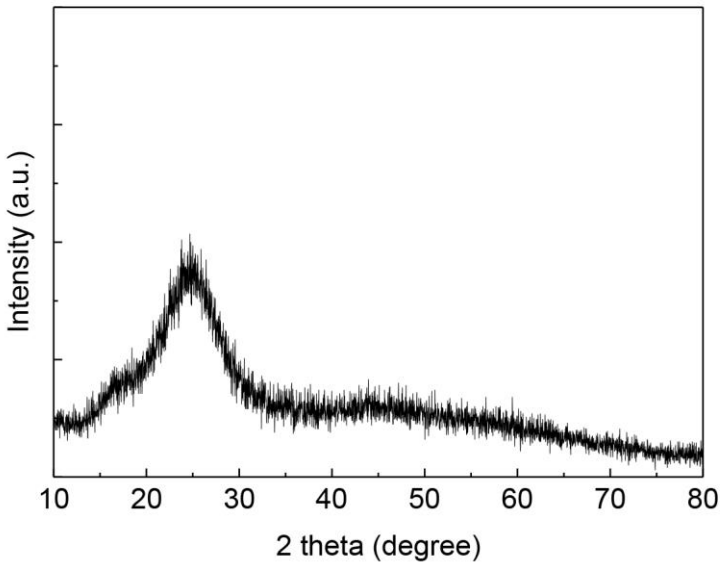

Supplementary Fig.13| XRD pattern of CMK-3/sulfur composites. The sulfur content is 60 wt% in the composites. No typical peaks of CMK-3 are shown in the pattern, proving the fully impregnation of sulfur powders.

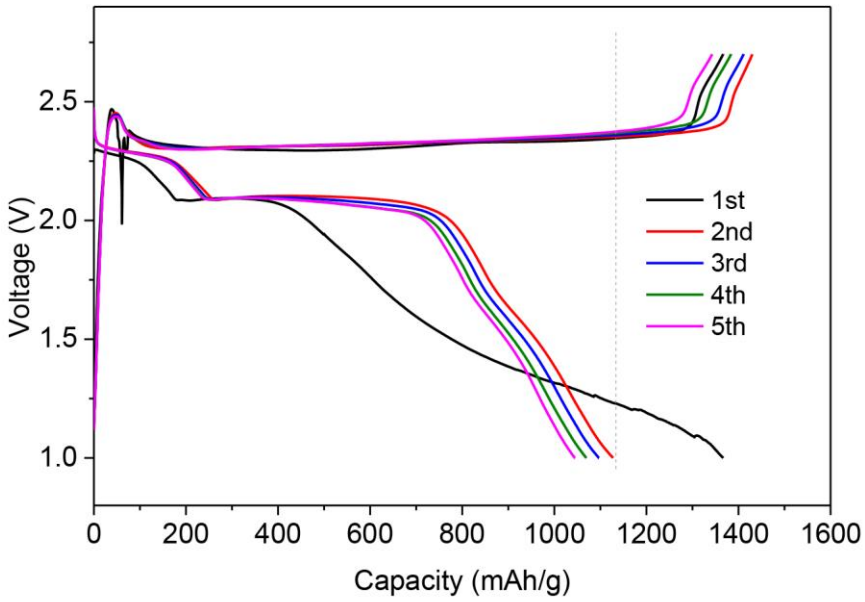

Supplementary Fig.14 | Discharge/charge curves of Li-S cells using liquid 2 *m* LiTFSI/DOL electrolytes at current density of 0.1 C.

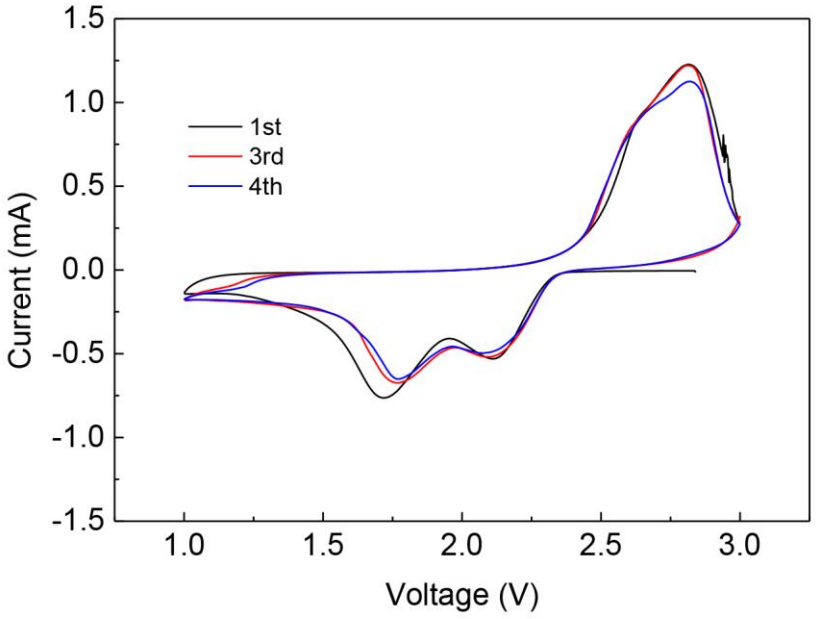

Supplementary Fig.15 | CV curves of Li-S batteries using polymer DOL electrolytes (0.5mM Al^{3+} + 2 *m* LiTFSI/DOL). The scanning rate is 0.1 mV/s.

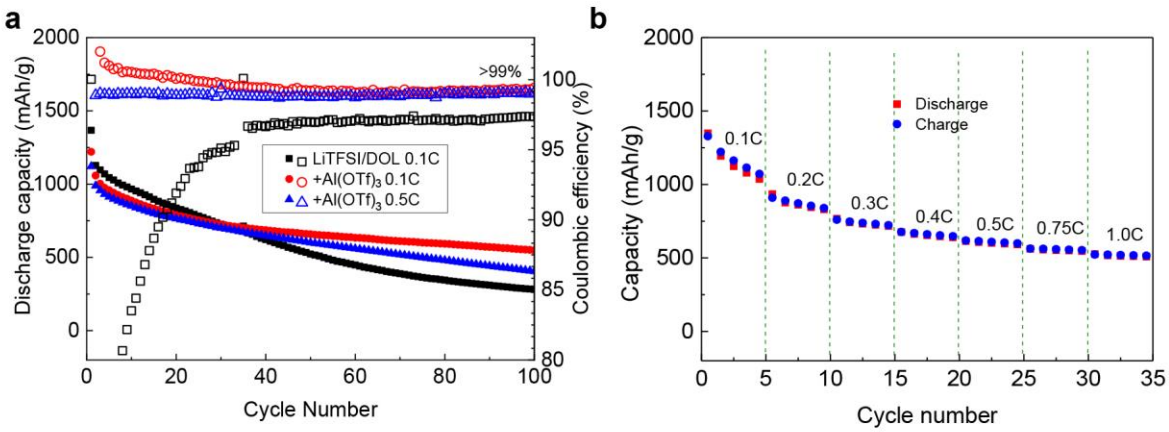

Supplementary Fig.16 | (a) Cycling performances and coulombic efficiencies of Li-S cells using liquid LiTFSI/DOL electrolyte and poly-DOL (Al^{3+} +LiTFSI/DOL) electrolyte. (b) Rate performance of Li-S cells using poly-DOL (Al^{3+} +LiTFSI/DOL) electrolyte

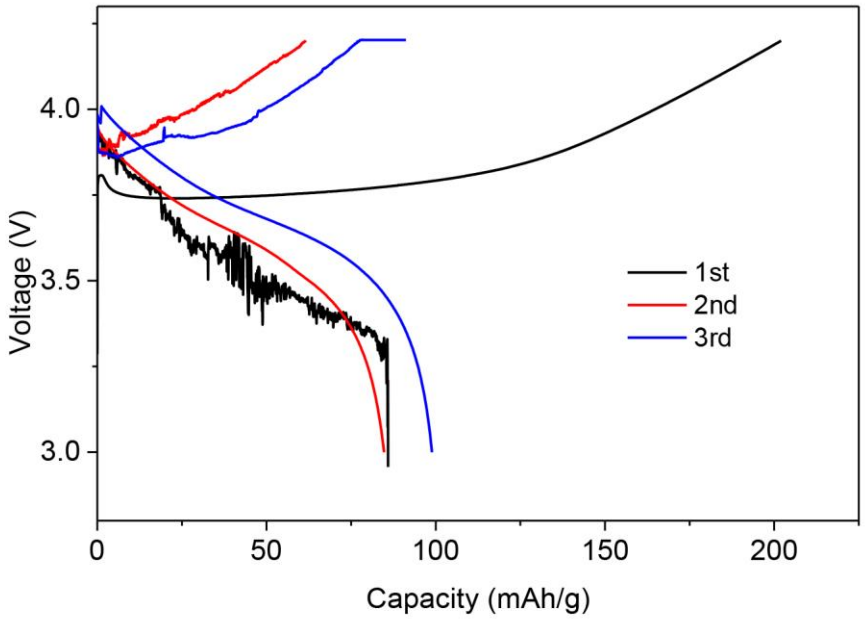

Supplementary Fig.17 | Discharge/charge curves of Li-NCM cells using liquid LiTFSI/DOL electrolytes (2 *m* LiTFSI/DOL) at current density of 0.1 C.

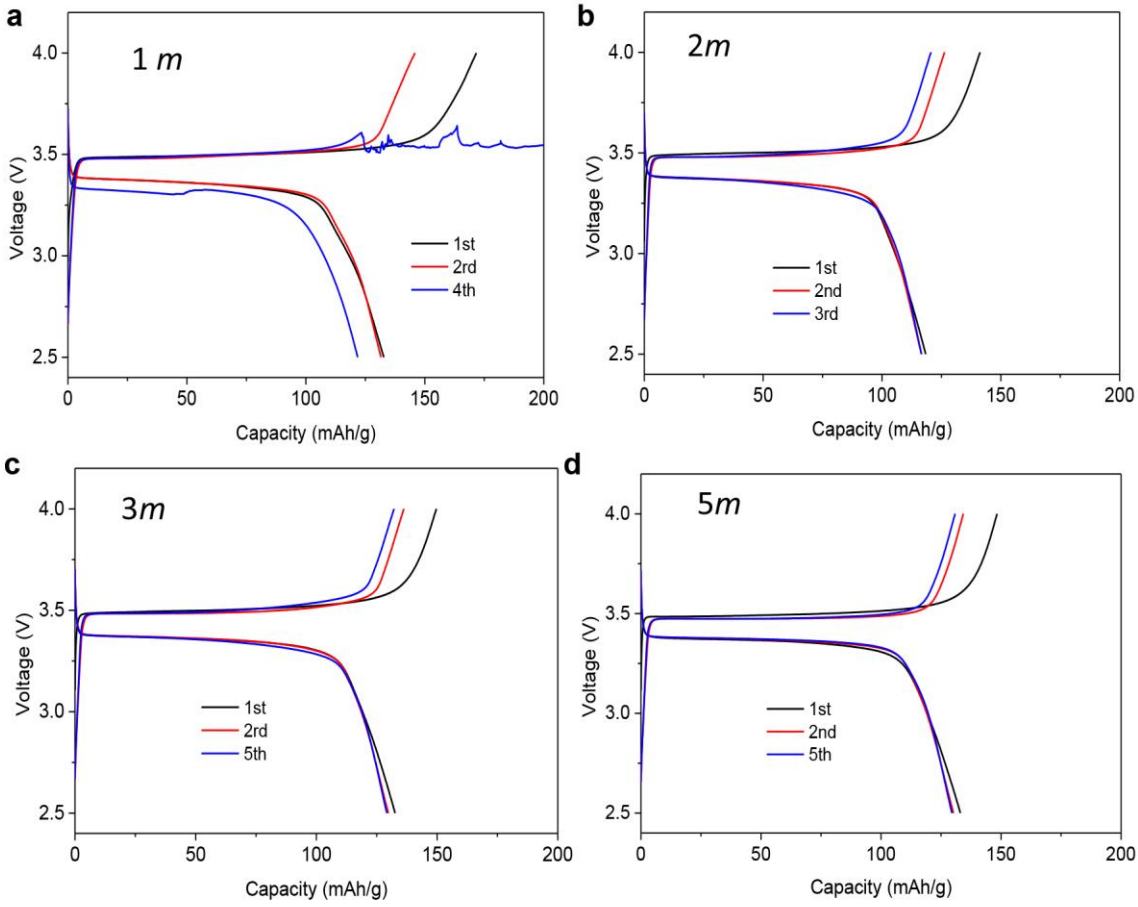

Supplementary Fig.18 | Discharge/charge profiles of Li-LFP cells using (a) 1 *m* LiTFSI-DOL; (b) 2 *m* LiTFSI-DOL; (c) 3 *m* LiTFSI-DOL; (d) 5 *m* LiTFSI-DOL liquid electrolyte.

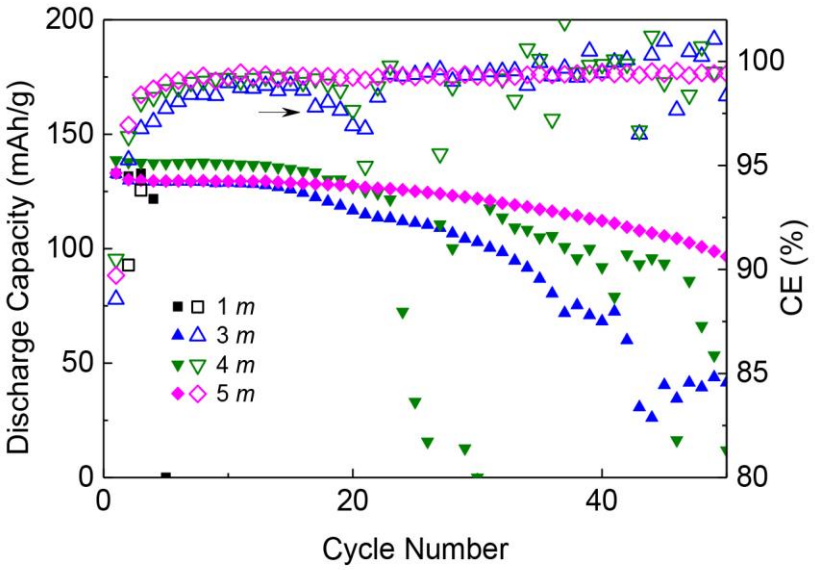

Supplementary Fig.19 | Cycling performances and coulombic efficiencies of Li-LFP cells using liquid LiTFSI-DOL electrolytes.

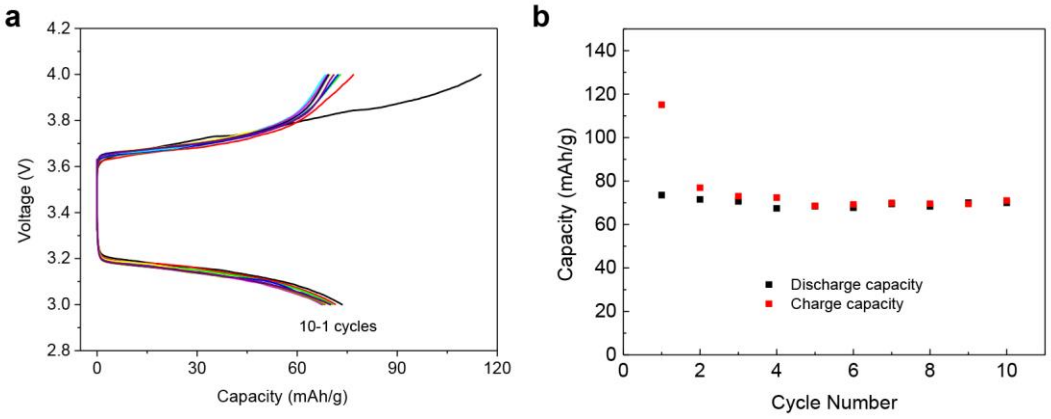

Supplementary Fig.20 | (a) Discharge/charge profiles and (b) Cycling performances of Li-LFP cells using an ex-situ made free-standing poly-DOL SPE. The current density is 0.1 C.

Supplementary Table 1 | GPC results, ionic conductivity and unpolymerized DOL ratio of prepared electrolytes using different concentrations of $Al(OTf)_3$

Sample	Mn (Daltons)	Mw (Daltons)	Polydispersity	Ionic conductivity (mS/cm)	DOL/ (DOL+ poly DOL)
2*m* LiTFSI/DOL				6.5	
0.2mM $Al(OTf)_3$	20K	59K	2.5	1.8	86%
0.5mM $Al(OTf)_3$	15K	37K	2.5	1.1	19%
1.0mM $Al(OTf)_3$	8.4K	15K	1.8	0.055	14%
5.0mM $Al(OTf)_3$	2.3K	3.3K	1.4	0.020	10%

Reference

1 Aurbach, D. *et al.* On the Surface Chemical Aspects of Very High Energy Density, Rechargeable Li–Sulfur Batteries. *J. Electrochem. Soc.* **156**, A694, (2009).

2 Aurbach, D., Youngman, O. & Dan, P. The electrochemical behavior of 1,3-dioxolane—LiClO4 solutions—II. Contaminated solutions. *Electrochimica Acta* **35**, 639-655, (1990).

3 Okada, M., Yamashita, Y. & Ishii, Y. polymerization of 1,2-Dioxolane. *Die Makromolekulare Chemie* **80**, 196-207, (1964).

4 Hagen, M. *et al.* In-Situ Raman Investigation of Polysulfide Formation in Li-S Cells. *J. electrochem. Soc.* **160**, A1205-A1214, (2013).

5 Wang, Z., Gao, W., Huang, X., Mo, Y. & Chen, L. Spectroscopic studies on interactions and microstructures in propylene carbonate-LiTFSI electrolytes. *J. Raman Spectroscopy* **32**, 900-905, (2001).

6 Kobayashi, M., Okamoto, I. & Tadokoro, H. Crystal vibrations of poly-1,3-dioxolane crystal form II and treatment of statistical errors due to uncertainties in the atomic positions. *Spectrochimica Acta Part A: Molecular Spectroscopy* **31**, 1799-1812, (1975).

7 Lu, Z., Yang, L. & Guo, Y. Thermal behavior and decomposition kinetics of six electrolyte salts by thermal analysis. *J. Power Sources* **156**, 555-559, (2006).